



**HAL**  
open science

## Medical potentialities of biomimetic apatites through adsorption, ionic substitution, and mineral/organic associations: three illustrative examples

Ahmed Al-Kattan, Farid Errassifi, Anne-Marie Sautereau, Stéphanie Sarda, Pascal Dufour, Allal Barroug, Isabelle dos Santos, Christèle Combes, David Grossin, Christian Rey, et al.

### ► To cite this version:

Ahmed Al-Kattan, Farid Errassifi, Anne-Marie Sautereau, Stéphanie Sarda, Pascal Dufour, et al.. Medical potentialities of biomimetic apatites through adsorption, ionic substitution, and mineral/organic associations: three illustrative examples. *Advanced Engineering Materials*, 2010, *Advanced Materials in Transportation / Materials For Health Care*, 12 (7), pp.1438-1656. 10.1002/adem.200980084 . hal-03474560

**HAL Id: hal-03474560**

**<https://hal.science/hal-03474560>**

Submitted on 10 Dec 2021

**HAL** is a multi-disciplinary open access archive for the deposit and dissemination of scientific research documents, whether they are published or not. The documents may come from teaching and research institutions in France or abroad, or from public or private research centers.

L'archive ouverte pluridisciplinaire **HAL**, est destinée au dépôt et à la diffusion de documents scientifiques de niveau recherche, publiés ou non, émanant des établissements d'enseignement et de recherche français ou étrangers, des laboratoires publics ou privés.



## Open Archive TOULOUSE Archive Ouverte (OATAO)

OATAO is an open access repository that collects the work of Toulouse researchers and makes it freely available over the web where possible.

This is an author-deposited version published in : <http://oatao.univ-toulouse.fr/>  
Eprints ID : 4650

**To link to this article** : DOI :10.1002/adem.200980084  
URL : <http://dx.doi.org/10.1002/adem.200980084>

**To cite this version :**

Al-Kattan, Ahmed and Errassifi, F. and Sautereau, Anne-Marie and Sarda, Stéphanie and Dufour, Pascal and Barroug, Allaland Dos Santos, Isabelle and Combes, Christèle and Grossin, David and Rey, Christian and Drouet, Christophe ( 2010)Medical potentialities of biomimetic apatites through adsorption, ionic substitution, and mineral/organic associations: three illustrative examples. *Advanced Engineering Materials*, vol. 12 (n° 7). pp. 1438-1656. ISSN 1438-1656

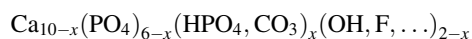
Any correspondance concerning this service should be sent to the repository administrator: [staff-oatao@inp-toulouse.fr](mailto:staff-oatao@inp-toulouse.fr).

# Medical Potentialities of Biomimetic Apatites through Adsorption, Ionic Substitution, and Mineral/Organic Associations: Three Illustrative Examples\*\*

By Ahmed Al-Kattan, Farid Errassifi, Anne-Marie Sautereau, Stephanie Sarda, Pascal Dufour, Allal Barroug, Isabelle Dos Santos, Christele Combes, David Grossin, Christian Rey and Christophe Drouet\*

*Biomimetic calcium phosphate apatites are particularly adapted to bio-medical applications due to their biocompatibility and high surface reactivity. In this contribution we report three selected examples dealing with mineral/organic interactions devoted to convey new functionalities to apatite materials, either in the form of dry bioceramics or of aqueous colloids. We first studied the adsorption of risedronate (bisphosphonate) molecules, which present potential therapeutic properties for the treatment of osteoporosis. We then addressed the preparation of luminescent Eu-doped apatites for exploring apatite/collagen interfaces through the FRET technique, in view of preparing “advanced” biocomposites exhibiting close spatial interaction between apatite crystals and collagen fibers. Finally, we showed the possibility to obtain nanometer-scaled apatite-based colloids, with particle size tailorable in the range 30–100 nm by controlling the agglomeration state of apatite nanocrystals by way of surface functionalization with a phospholipid moiety. This paper is aimed at illustrating some of the numerous potentialities of calcium phosphate apatites in the bio-medical field, allowing one to foresee perspectives lying well beyond bone-related applications.*

Apatitic calcium phosphates are major constituents of vertebrate hard tissues. In particular, bone mineral is composed of non-stoichiometric nanocrystalline apatites, which generally respond to the chemical formula:



where  $0 \leq x \leq 2$ . One of the specificities of the apatite structure is its ability to accommodate many types of mineral (or small organic) ions as well as large amounts of vacancies.<sup>[1]</sup> Nanocrystalline non-stoichiometric calcium phosphate (CaP) apatites, both biological or synthetic, were found to involve ions located in chemical environments which did not correspond to regular apatite, referred to as “non-apatitic.”<sup>[2,3]</sup> These

[\*] Dr. C. Drouet, A. Al-Kattan, Dr. S. Sarda, Dr. C. Combes  
Dr. D. Grossin, Prof. C. Rey  
Université de Toulouse – CIRIMAT Carnot Institute, CNRS/  
INPT/UPS, ENSIACET 4 allée Emile Monso, BP 44362,  
31432 Toulouse Cedex 04, France  
E-mail: christophe.drouet@ensiacet.fr  
F. Errassifi, Prof. A. Barroug  
LPCME, Département de Chimie, Faculté des Sciences  
Semailia – UCA Bd Prince My Abdellah, BP 2390, 40000  
Marrakech, Morocco  
Prof. A. M. Sautereau  
Université de Toulouse – CIRIMAT Carnot Institute, CNRS/  
INPT/UPS, Université Paul Sabatier, Faculté de Pharmacie  
118 route de Narbonne, 31062 Toulouse Cedex 04, France

Dr. P. Dufour  
Université de Toulouse – CIRIMAT Carnot Institute, CNRS/  
INPT/UPS, Université Paul Sabatier  
LCMIE, 118 route de Narbonne, 31062 Toulouse Cedex 04,  
France  
Dr. I. Dos Santos  
Laboratoire de pharmacie galénique et biopharmacie, Univer-  
sité Victor Segalen Bordeaux 2, 146 rue Léo Saignat, 33076  
Bordeaux Cedex, France

[\*\*] Acknowledgements, This work was supported in part by the Franco-Moroccan Volubilis Integrated Action (MA/05/122). The authors are also grateful to Procter and Gamble for generously providing risedronate samples, and thank Serge Mazeres (IPBS laboratory, France) for technical assistance with spectrofluorimetry.

non-apatitic chemical environments form a surface hydrated layer on such biomimetic apatite nanocrystals, and the extent of this layer was shown in these works to be directly dependent on the conditions of formation of the crystals. A high ion mobility within this layer was evidenced by way of surface ion exchanges carried out within very short periods of time (often under 20 min)<sup>[3]</sup> and is thought to explain the exceptional surface reactivity<sup>[4]</sup> of nanocrystalline apatites.

Bulk ionic substitutions (leading to solid solutions) are also of interest from an applied viewpoint insofar as they confer an additional property to the apatite matrix. In this regard, the possibility to convey luminescence properties to CaP apatites appears as a particularly attractive option due to an increasing demand for non-toxic biocompatible systems for medical imaging applications. Luminescent apatites can indeed be obtained by substituting part a few at% of the calcium ions by rare earth elements such as europium,<sup>[5]</sup> which was mostly shown in the case of well-crystallized apatites obtained at high temperatures.

Adsorption phenomena also represent an important physico-chemical aspect to take into account. The adsorption of proteins is for example considered to play a determining role in mineralized tissues *in vivo*.<sup>[6]</sup> Surface functionalization with organic molecules such as drugs (e.g., antibiotics...) or other biomolecules of interest (e.g., growth factors...) also opens large opportunities in view of medical treatments: for example in the field of bone repair for activating bone tissue regeneration or for limiting osteoclastic resorption. Several bone proteins such as osteocalcin, osteopontin, as well as biomolecules like albumin, or else phospholipids, among others, have been shown to adsorb on and interact strongly with apatite.<sup>[7]</sup> In the biomaterials field, as previously mentioned for mineral ions, some organic molecules interacting with calcium phosphates are thought to play a crucial role in the recruitment and expression of cells, and that they are strongly involved in the biointegration of implants.<sup>[8]</sup> Considering the treatment of bone diseases, some bone-adsorbing molecules like bisphosphonates have been used to control bone turnover.<sup>[9]</sup> Indeed, their biological activity has been shown recently to be correlated with their adsorption properties.<sup>[10]</sup>

The aim of this paper is to illustrate and comment some of the possibilities offered by calcium phosphate apatites, due to their intrinsic properties and exploiting their excellent biocompatibility. We report on the incorporation of Eu<sup>3+</sup> ions into nanocrystalline apatites for conveying intrinsic luminescence properties in the view of exploring the interface formed with autofluorescent (or dye-doped) biopolymers/proteins such as collagen. We also examine two types of surface modifications on CaP apatites: the adsorption (and desorption) of a bisphosphonate drug (residronate) used for the treatment of osteoporosis, and the functionalization of apatite crystals with a phospholipid moiety, 2-aminoethylphosphate (AEP), in view of controlling the agglomeration state of apatite, for preparing colloidal apatite nanoparticles intended for intracellular drug delivery or (in the case of luminescent systems) for intracellular imaging.

## Experimental

### Synthesis Protocols

The risedronate adsorption experiments were performed on a calcium phosphate apatite exhibiting a chemical composition close to stoichiometry, referred to as hydroxyapatite "HA." This sample was prepared by double decomposition between a calcium nitrate solution and an ammonium phosphate solution (Alfa Aesar, reagent grade). A starting stoichiometric molar ratio of Ca/P = 1.67 was used. The phosphate solution was added dropwise, over 3 h, into the calcium solution maintained at 90 °C under continuous stirring; the pH of the suspension was around 10. After filtration, the precipitate was washed with deionized water and freeze-dried.

The luminescent (non-colloidal) apatite samples were prepared by precipitation after mixing at moderate temperature (in the range 37–100 °C) an aqueous solution of calcium and europium nitrates and an aqueous solution of ammonium hydrogenphosphate. Typically, a total concentration of 3.12 M of calcium and europium nitrates was mixed with 1.04 M of ammonium hydrogenphosphate (total volume 12.5 mL) at a starting pH set to 9 by addition of ammonia. Increasing Eu/(Ca + Eu) mole ratios in the precipitating solution were investigated. The obtained precipitates were filtered, washed with deionized water and freeze-dried. The association of such luminescent apatite (europium-doped apatite) with collagen macromolecules (type I from bovine Achilles tendon, Sigma-Aldrich) was investigated either by mechanically mixing the Eu-doped apatite powder and the collagen fibers (in an apatite-to-collagen weight ratio of 90:10), or by dispersing the collagen fibers in the phosphate solution during Eu-doped apatite synthesis at 37 °C for 2 h (leading to Eu-doped apatite precipitating within a suspension of collagen fibers).

The colloidal apatite samples were synthesized at temperatures in the range 80–100 °C for 16 h, under alkaline pH close to 9, by precipitation from calcium nitrate and ammonium hydrogenphosphate solutions in the presence of a biocompatible dispersing agent (phospholipid moiety): 2-aminoethylphosphate, or "AEP" (Sigma-Aldrich) introduced in the calcium solution. The starting AEP/(Ca + Eu) molar ratio used in this work was selected in the range 0–1. Dialysis in water was used as the purifying method for apatite colloids, using a cellulose tubular membrane (molecular weight cutoff: 6000–8000 Da). The pH value of the colloids was adjusted, when needed, to physiological value in a subsequent step. When mentioned in the text, europium ions were added in the calcium solution (with a Eu/(Ca + Eu) ratio of 1.5%) prior to precipitation, in view of preparing luminescent AEP-stabilized apatite colloids.

### Risedronate Adsorption and Desorption Experiments

The risedronate sample used in this study, [1-hydroxy-2-(3-pyridinyl)ethylidene] bisphosphonic acid] monosodium

hemipentahydrate salt, was generously provided free of charge by Procter & Gamble Pharmaceuticals.

The adsorption experiments were carried out at physiological temperature and pH ( $T = 37 \pm 1^\circ\text{C}$ ;  $\text{pH} \approx 7.4$ ) by equilibrating 50 mg of nearly stoichiometric HA prepared as mentioned above, with 5 mL of risedronate solutions (concentration ranging from 0 to 5.7 mM in 1 mM potassium chloride aqueous solution). The suspensions were sonicated for a few minutes and incubated for 2 h without stirring. After centrifugation at 15 000 rpm, the supernatants obtained were retained by a membrane filter (pore size 0.2  $\mu\text{m}$ ) and characterized.

Desorption tests were performed by replacing the supernatants obtained after centrifugation with the same volume of potassium chloride solution previously equilibrated with HA powder but without adsorbate. The sediments were re-dispersed and incubated for 2 h; the suspensions were centrifuged again and the amount of risedronate in the supernatants was analyzed.

#### Characterization Techniques

The chemical composition of the apatites synthesized was determined using several complementary techniques. Complexometry with ethylene-diamine-tetraacetic acid (EDTA) was used for the determination of calcium in the europium-free samples. The Ca and Eu contents in europium-containing samples were evaluated by ion-coupled plasma spectroscopy (ICP-MS) on a Perkin Elmer Elan 6000 apparatus. The amount of calcium ions released upon adsorption was measured by atomic absorption spectrophotometry (Unicam model 929). The phosphate content of all apatite samples was drawn from spectrophotometry measurements at  $\lambda = 460$  nm after formation of yellow phospho-vanado-molybdcic acid [11].

For risedronate adsorption experiments, the risedronate concentration in solution was determined by UV absorption spectroscopy at 262 nm (Hawlett Packard 8452 Diode Array spectrophotometer).

Nitrogen titrations were performed, for AEP-containing samples, by elemental microanalysis using a Perkin-Elmer 2400 II analyzer.

The crystal structure of the samples was identified by powder X-ray diffraction (XRD) using an Inel diffractometer CPS 120 and the monochromatic  $\text{CoK}_\alpha$  radiation ( $\lambda_{\text{Co}} = 1.78892 \text{ \AA}$ ).

Fourier transform infrared (FTIR) analyses were carried out on a Thermo Nicolet 5700 spectrometer in the wavenumber range 400–4000  $\text{cm}^{-1}$ , with a resolution of 4  $\text{cm}^{-1}$ , using the KBr pellet method.

The specific surface area,  $S_w$ , of the samples was determined from the BET method (nitrogen adsorption) on a Nova 1000 Quantachrome apparatus.

Granulometry data (determination of hydrodynamic radius) for the colloidal particles were obtained by dynamic light scattering (DLS) using a Malvern Nanosizer ZS apparatus ( $\lambda = 630$  nm). Zeta potential measurements were

run on the same apparatus with an adapted electrophoretic mobility cell.

Transmission electron microscopy (TEM) micrographs were recorded in the secondary electron mode on a JEOL JEM-1011 microscope set up at an acceleration tension of 100 kV.

Fluorescence properties for apatite–collagen associations were investigated with an Aminco SPF 500C spectrofluorimeter. A sample holder adapted to the analysis of solid state substrates fixed on a microscope glass plate was used.

#### Results and Discussion

As mentioned in the introduction section, the apatite structure is capable of accommodating many substituents and vacancies, which leads to the possibility to tailor to some extent the chemical composition of apatitic compounds in view of pre-determined applications. Moreover, the ionic nature of apatite compounds leads to the exposure of both anions and cations on the surface of the crystals, thus enabling to anticipate possible interactions with (bio)molecules exhibiting charged end-groups such as carboxylate, phosphate, or phosphonate functions for instance.

The following sections are dedicated to illustrate three types of such possibilities:

- the adsorption on apatite of a bisphosphonate salt used in the treatment of osteoporosis,
- the incorporation of luminescent  $\text{Eu}^{3+}$  ions in apatites and the exploration by Förster (or “Fluorescence”) resonance energy transfer (FRET) of interfaces with autofluorescent collagen,
- and the functionalization of apatite colloidal nanoparticles with a phospholipid moiety in view of the preparation of new nanometer-scale intracellular drug carriers or luminescent nanoprobes.

#### Surface Adsorption of Risedronate Molecules

Bisphosphonate molecules have lately raised a great interest for the treatment of bone-related pathologies accompanied with poor mineralization condition, such as osteoporosis. This section addresses from a physico-chemical point of view the interaction of apatite crystals with one such bisphosphonate, risedronate, with the view to better understand the type of interaction existing between this therapeutic molecule and the surface of apatite crystals.

This study was run on an HA compound, referred to as HA. This sample was found to exhibit an XRD pattern and FTIR spectrum characteristic of a well-crystallized calcium phosphate apatite. The specific surface area of HA was 59  $\text{m}^2\text{g}^{-1}$ . Chemical analyses led to a Ca/P ratio of 1.64, characteristic of nearly stoichiometric HA. No other crystalline phase was detected by XRD after risedronate adsorption.

The adsorption isotherm of risedronate at pH 7.4 and 37 °C onto the HA prepared was obtained by plotting the evolution of the amount of risedronate adsorbed by HA, as a function of its equilibrium concentration in solution (Fig. 1). The isotherm

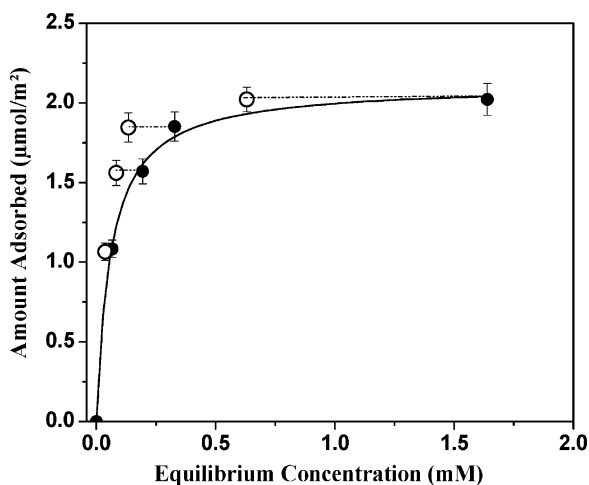


Fig. 1. Adsorption (plain symbols) and desorption (open symbols) isotherms of risedronate on HA at pH = 7.4 and T = 37 °C; the dashed lines indicate that no risedronate desorbs upon dilution.

was found to be Langmuirian with a good correlation factor ( $r^2 \geq 0.99$ ), and the plateau ( $2.1 \mu\text{mol m}^{-2}$ ) was reached at relatively low risedronate concentrations. These findings point out a high affinity between risedronate molecules and apatite. Similar adsorption characteristics were reported for the interaction of others bisphosphonates on calcium phosphates.<sup>[12]</sup> From the Langmuir equation, we can calculate the parameters of adsorption: the amount of risedronate adsorbed at saturation ( $2.31 \pm 0.06 \mu\text{mol m}^{-2}$ ) and the affinity constant of risedronate for the apatitic surface ( $7.27 \pm 3.64 \text{ L mmol}^{-1}$ ). Adsorption parameters depend on several factors such as pH, temperature or nature of the apatitic support, and thus the determination of such parameters contributes to better understand the interaction between bisphosphonates molecules and bone mineral.

Desorption results obtained by decreasing the risedronate concentration in the solution by diluting with a potassium chloride solution (Fig. 1) suggested that the process is irreversible with respect to dilution in the range of concentrations examined. These findings thus indicate that the amount of risedronate adsorbed is not altered by dilution of the adsorption solution or even upon washing of the samples.

Very interestingly, the analysis of the suspensions obtained after adsorption revealed that the binding of (negatively-charged) risedronate ions onto the HA surface was accompanied by the release of phosphate ions in the solution, pointing out a more complex process than simple surface grafting. The variation of the concentration of phosphate ions released in solution as a function of the amount of adsorbed risedronate is plotted in Figure 2. As can be seen, the amount of phosphate released increases linearly with respect to the uptake of risedronate ions, whereas the adsorption of risedronate has only a weak influence on the calcium content of the solution. This observation thus strongly suggests that risedronate molecules substitute for phosphate ions localized on the apatite surface. Considering that the dissolution of HA

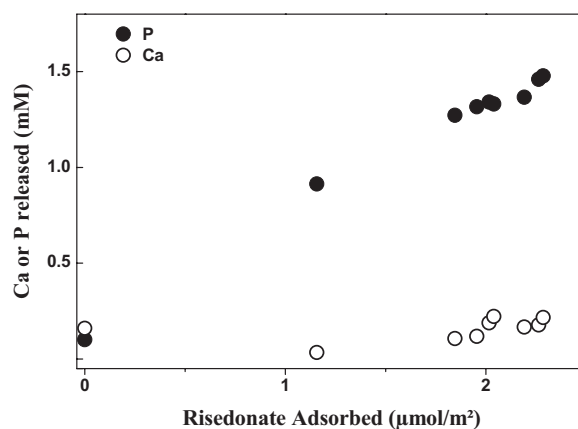


Fig. 2. Variation of the phosphate and calcium concentrations in the solution versus the amount of risedronate adsorbed.

in our system is congruent (i.e., that the Ca/P ratio is the same in the solid and the solution:  $\text{Ca/P} = 1.64$ ), the calculations indicate that the adsorption reaction corresponds to an ion exchange process between risedronate molecules in solution and phosphate ions from the apatite surface, with a one-to-one substitution process (except for the first point of the isotherm), which can thus be described by the reaction:



From this reaction, it appears that the exchange process is not only related to the concentration in the solution of the “adsorbing” risedronate ions, but also to that of the  $\text{PO}_4^{3-}$  ions that are being exchanged. From reaction (1), one can then write the equilibrium constant:

$$k = \frac{[\text{PO}_4^{3-}]N_e}{([\text{Ri}^{3-}](N_m - N_e))} \quad (2)$$

where  $N_e$  is the amount of  $\text{Ri}^{3-}$  ions taken up by the apatite sample,  $[\text{Ri}^{3-}]$  the equilibrium risedronate concentration in the solution,  $[\text{PO}_4^{3-}]$  the equilibrium phosphate concentration, and  $N_m$  the total number of exchange sites. This equation can then be transformed into a Langmuir-like isotherm equation by extracting  $N_e$ , leading to:

$$N_e = N_m k ([\text{Ri}^{3-}] / [\text{PO}_4^{3-}]) / (1 + k ([\text{Ri}^{3-}] / [\text{PO}_4^{3-}])) \quad (3)$$

Indeed, in this equation, the equilibrium concentration of “adsorbate” in a traditional Langmuir equation is simply replaced by the concentration ratio  $[\text{Ri}^{3-}] / [\text{PO}_4^{3-}]$  in the exchange reaction equilibrium.

Additionally, it should be noted that although the solubility equilibrium of HA would lead to a decrease of the free calcium ions in the solution, this is not observed and the stability (and even the slight increase) of the calcium content with the increase in risedronate in solution may be interpreted as an indication for the probable formation of ion pairs or complexes between risedronate molecules and calcium ions in solution.

The above findings implicate that risedronate molecules are capable of being fixed in a strong way on the surface of apatite crystals, implying an ion exchange mechanism, and cannot be displaced by simple dilution. These results thus make it possible to anticipate the preparation of “superior” bisphosphonate-enriched apatite bioceramics for treating osteoporosis-like conditions (localized implantation in high-fracture-risk areas) while limiting the uncontrolled desorption/release of the drug throughout the organism.

This example, considering the different equilibria involved (mineral dissolution, adsorption, complex formation), shows that the interaction of apatite with organic molecules/drugs may not be straightforwardly described by a “simple” adsorption model, and that the main driving force seems to be an ion-exchange process involving the replacement of mineral ions of the apatite surface by molecular ions from the solution. This can also be the case for other molecules exhibiting charged end-groups. The process of adsorption can be related with an alteration of the mineral ion concentration in solution and, inversely, mineral ions in solution were found to interact strongly with the adsorption. The observation of such ions exchange interactions needs a precise evaluation of the amount adsorbed and of the mineral ion content of the solution when investigating adsorption phenomena onto apatite compounds, so that the possible release of phosphate or calcium ions during adsorption experiments should probably always be monitored.

### Eu<sup>3+</sup>-Doped Luminescent Apatites for Exploring Interfaces of Bio-Medical Interest

The incorporation of luminescent rare-earth elements such as europium presents a potential interest for the exploration of interfaces within multi-material systems where another part of the system also exhibits fluorescence capabilities. Indeed, in this conjecture, techniques based on FRET may then be advantageously exploited for assessing whether the interface between the two luminescent subparts involves a close spatial interaction or not. This is linked to the basic principles of the FRET process which exhibits a decreasing intensity when the distance “*r*” separating both chromophores increases, following a “ $1/r^6$ ” mathematical law:<sup>[13]</sup> the detection of a significant FRET signal is indeed a mark of the nanometer-range proximity of the two chromophores. This aspect of “spatial vicinity” between two subparts of a system is then informative on the existence and the “quality” of the interface, which is an important concern when exploring for example new synthesis routes for the production of advanced biocomposites (e.g., for bone filling application). The main interest of FRET-based techniques is the possibility to get information down to scales of about 5–10 nm while the classically-used observation techniques are often limited to about an order of magnitude higher.

This aspect would for example be applicable to interfaces between luminescent apatite crystals (as the “acceptor” of the FRET process) and collagen (as the “donor”), the latter being

indeed known to exhibit autofluorescence properties.<sup>[14]</sup> For this purpose, the preparation of luminescent apatite compounds is therefore needed. In this work, we addressed more specifically this physico-chemical aspect by doping calcium phosphate apatites with europium ions during the synthesis process. Europium was selected in this study due to several interesting properties of this element such as rather simple excitation/emission spectra with thin lines, long luminescence lifetime, low toxicity, and excitability in the emission domain of collagen.

The possibility to incorporate europium in the apatite structure was studied in several works.<sup>[15]</sup> However, the vast majority of such literature reports dealt with apatite compounds synthesized at high temperature (>1000 °C) and therefore exhibiting a high degree of crystallinity that is far from the one found in biological apatites. In contrast, we have prepared in the present work a series of apatite compounds by moderate-temperature soft chemistry routes with the objective to obtain more reactive apatite crystals, with crystallinity states closer to those found in bone mineral.

Several Eu-doped apatite samples were prepared with increasing Eu contents corresponding to starting ratios Eu/(Ca + Eu) in the range 0–2 mol%. XRD and FTIR analyses of the obtained samples showed all the characteristic features of moderately-well crystallized apatites, and no indication on the presence of secondary phases was evidenced. Figure 3 reports for example the evolution of the XRD patterns corresponding to 0, 1, 1.5, and 2% Eu in the starting mixture. Only diffraction lines attributable to a single apatite phase were found and indexed (after ICDD-JCPDS datasheet 09-432). Slight variations in the XRD patterns could however be noticed such as a decrease in the resolution of XRD lines upon increasing Eu doping rates, which is especially visible in the 2θ range 34–42°. This evolution was quantified by measuring for each composition the “crystallinity index,”  $I_{\text{cryst}}$  determined from the resolution of XRD line (300) using the method proposed by

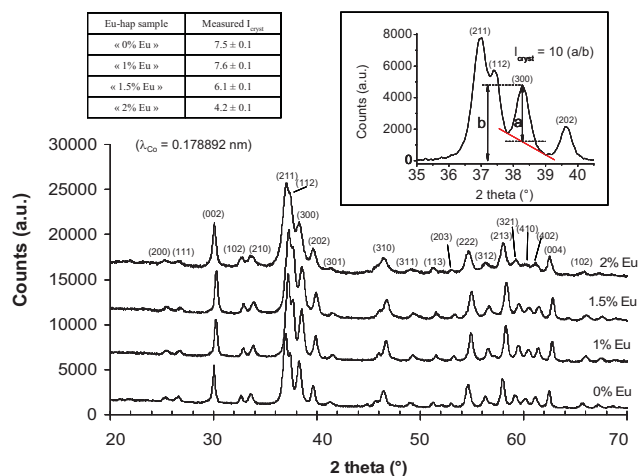


Fig. 3. XRD patterns for Eu-doped apatite samples (non-colloidal) with varying Eu doping rates. Insets: calculation scheme for crystallization index  $I_{\text{cryst}} = 10(a/b)$ , and measured values for  $I_{\text{cryst}}$ .

Table 1. Compositional data for the prepared Eu-doped apatite compounds.

Starting Eu/(Ca + Eu) ratio in solution (%)	(Ca + Eu)/P ratio in solid <sup>[a]</sup>	Cationic contents in 100 mg of solid		Experimental Eu/(Ca + Eu) ratio in solid (%)	Calculated <sup>[b]</sup> Eu/(Ca + Eu) ratio in solid (%)
		Ca (mmol)	Eu (mmol)		
0	1.66 ± 0.01	0.951 ± 0.029	0	0	0
1.000 ± 0.005	1.60 ± 0.01	0.903 ± 0.027	0.017 ± 0.001	1.9 ± 0.2	2.04 ± 0.13
1.500 ± 0.005	1.61 ± 0.01	0.882 ± 0.026	0.026 ± 0.001	2.9 ± 0.2	3.03 ± 0.13
2.000 ± 0.005	1.57 ± 0.01	0.838 ± 0.025	0.036 ± 0.001	4.1 ± 0.1	4.05 ± 0.13

[a] Evaluated from chemical analyses;

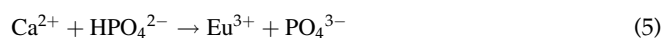
[b] assuming all the Eu<sup>3+</sup> ions present in the starting mixture have reacted.

Bartsiokas and Middleton,<sup>[16]</sup> and schematized on the inset of Figure 3. The measured values of  $I_{\text{cryst}}$  were found to decrease noticeably upon europium incorporation (from about  $7.5 \pm 0.1$  down to  $4.2 \pm 0.1$ ). This evolution quantifies a noticeable decrease in crystallinity state upon Eu doping. It may be linked to an inhibiting crystal growth effect due to the presence of Eu<sup>3+</sup> ions, likely to stabilize the non-apatitic surface layer over the apatitic core, and to increase the amount of defects in the overall structure.

Some compositional characteristics of the doped apatite samples (Eu: 0–2%, 100 °C for 16 h, pH ≈ 9) are given in Table 1. The (Ca + Eu)/P molar ratio of the solids was evaluated from chemical titrations of Ca, Eu, and phosphate and tends to indicate that the incorporation of europium is accompanied by a slight decrease in this ratio, pointing out an increase in the number of ionic vacancies in the solids. These results are in agreement with the XRD data previously mentioned. Table 1 also indicates that the europium doping rates found in the solids are greater than the Eu doping rates in the starting mixtures, with a multiplying factor close to 2. These findings point out the preferential incorporation of europium ions over calcium ions despite rather similar ionic radii (1.00 Å for Ca<sup>2+</sup>, 0.95 Å for Eu<sup>3+</sup>).<sup>[17]</sup> In order to shed some light on this aspect, so-called “theoretical” Eu/(Eu + Ca) molar ratios were calculated (see Table 1) assuming the incorporation of all Eu<sup>3+</sup> ions initially present in the starting mixtures. Interestingly, the resulting calculated ratios were found to be extremely close to the experimental ones, thus confirming the occurrence of a preferential incorporation of Eu<sup>3+</sup> ions in the apatite lattice in our preparation conditions. This effect could for example be linked to a more energetic Eu–O bond as compared to Ca–O. Indeed, some studies have pointed out the high affinity of europium ions for oxygen in apatite matrices,<sup>[18]</sup> leading to pseudo-covalent bonds, which is also consistent with the +3 charge of the ion as compared to that of calcium.

Several Eu<sup>3+</sup> → Ca<sup>2+</sup> bulk substitution mechanisms can be considered in such apatites: in the absence of monovalent or tetravalent ions in the medium, as is the case here, the following schemes may a priori be considered (a square represents an ionic vacancy in the corresponding crystal-

lographic site):



or a combination of two or more of such mechanisms. At this stage, none of these mechanisms can be a priori privileged or discarded. Moreover, two or more of these mechanisms may come into play simultaneously; and the increase of Eu doping rate might also lead from one preferred mechanistic scheme for low doping rates to another preferential mechanism at higher Eu contents. These aspects will be further investigated in future studies.

The above results showed the possibility, with our synthesis conditions, to incorporate Eu<sup>3+</sup> ions into the apatite structure (up to at least 2 mol% relative to calcium) while retaining a wet chemistry preparation process. It was thus interesting to check at this point whether an FRET signal could be detected for apatite–collagen systems. Interestingly enough, among the two types of Eu-apatite/collagen associations tested in this work, the first protocol based on simple mechanical mixture did not lead (Fig. 4) to any europium-linked emission upon excitation at 340 nm (excitation domain of collagen exclusively). In contrast, the second way of Eu-apatite and collagen association involving the precipitation (at 37 °C for 2 h) of apatite in the presence of collagen, led to two emission bands around 592 nm (minor) and 616 nm (major), as shown in Figure 4. These two bands are characteristic of the emission bands of europium relative to the de-excitation transitions  ${}^5\text{D}_0 \rightarrow {}^7\text{F}_1$  and  ${}^5\text{D}_0 \rightarrow {}^7\text{F}_2$ , respectively,<sup>[19]</sup> despite an excitation in the exclusive collagen domain. These findings thus tend to show that, for a precipitation in the presence of collagen, the Eu<sup>3+</sup> ions incorporated in the apatite structure were successively subjected to excitation and de-excitation (emitting the observed photons), and this phenomenon would then be

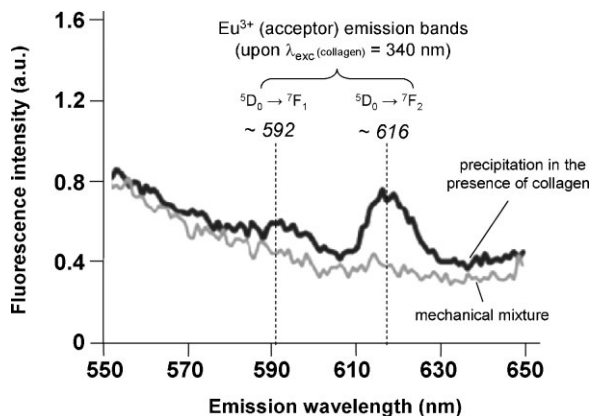


Fig. 4. Luminescence properties (FRET) for two types of Eu-doped (2 mol%) apatite/collagen associations: mechanical mixture and apatite precipitation in the presence of collagen.

characteristic of a FRET signal between the collagen donor and the  $\text{Eu}^{3+}$  accepting ions.

This observation, therefore, insinuates that this second type of association led to apatite crystals in close spatial interaction with the collagen molecules. The analysis by XRD and FTIR of the apatite crystals precipitated (for 2 h at  $37^\circ\text{C}$ , see Fig. 5) in the presence of collagen led to data very close to the ones obtained without collagen. For example, on the FTIR spectrum the bands characteristic of apatite can be seen (phosphate,  $\text{OH}^-$  and minor carbonate bands as shown) as well as some amide bands from collagen. The presence of collagen therefore did not lead to major differences in the crystallization of apatite nanocrystals (mean crystallite size from Scherrer's formula: 17 nm length and 6 nm width), but may have played a role of nucleating substrate. This preparation route would thus appear as a promising method for the elaboration of advanced biocomposites susceptible of exhibiting homogeneous and optimized macro- and microscopic properties. In contrast, the absence of europium emission for the simple mechanical mixture between collagen fibers and apatite

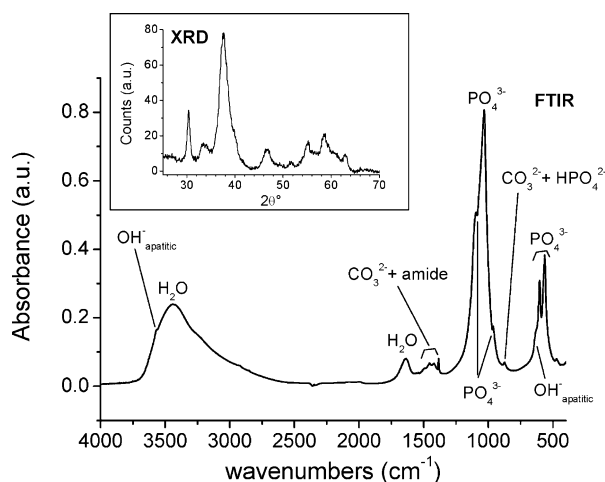


Fig. 5. FTIR spectrum and XRD pattern (inset) for apatite precipitated in the presence of suspended collagen fibers (2 h at  $37^\circ\text{C}$ ).

crystals unveils the poor quality of the apatite–collagen interface in such a system, thus suggesting to avoid preparation routes based on sole mechanical mixture.

#### Functionalization with a Phospholipid Moiety for Controlling Agglomeration

The agglomeration of apatite particles is a common phenomenon, especially when dealing with nanocrystalline apatite crystals exhibiting large surface areas. In fact, agglomeration (like hydration processes) is a simple way to limit the surface energy of many ionic solids. The aggregation of adjacent nanocrystals for forming agglomerates is not a problematic concern per se when the apatite compound is intended for bone repair applications where consolidated ceramics are generally needed. However, the agglomeration of apatite nanocrystals into micron-size (or larger) aggregates becomes a critical issue when intracellular applications are envisioned, since the size of the host cells (up to a few tens of microns) has then to be taken into account. For example in view of intracellular drug delivery, apatite particles will require surface modifications so as to remain in the nanometer range (typically under 100 nm), while retaining the biocompatibility of the system. One obvious way to reach this anti-agglomeration effect is by functionalizing, during precipitation, the surface of apatite nanocrystals with biocompatible molecules capable of both (i) interacting advantageously/energetically with apatite (good binding properties) and (ii) enabling some steric hindrance (or better electro-steric) for inhibiting in a stable way the union of neighboring crystals, leading to colloidal suspensions.

This topic has been investigated here for apatite suspensions prepared from easily handled ionic salts, by following the effect of surface functionalization with the phospholipid moiety AEP:  $\text{NH}_3^+ - \text{CH}_2 - \text{CH}_2 - \text{OP}(\text{O})(\text{O}^-)_2$ . In addition to its biocompatibility, this molecule (already present on the membrane of human cells)<sup>[20]</sup> was selected due to the presence of a phosphate group on one side of the molecule (enabling to predict good interacting properties with apatite) and of a charged ammonium end-group on the other side of the molecule (for electrostatic repulsion of adjacent particles).

In this work, AEP was added in various proportions during apatite precipitation. The suspensions prepared (in the temperature range  $80\text{--}100^\circ\text{C}$ ) from starting AEP/Ca molar ratios greater than 0.4 were found to be stable translucent colloids, whereas for lower ratios opaque suspensions were obtained and a sedimentation rapidly occurred (within an hour). In all cases studied, including in the presence of europium with starting Eu molar contents in the range 0–2% (relative to calcium), the apatitic nature of the particles in suspension was assessed by both FTIR and XRD analyses. By FTIR, an additional band was observed at  $754\text{ cm}^{-1}$  which is attributable to  $\text{Ca}(\text{AEP})_2$  complexes,<sup>[21]</sup> thus revealing interactions between the phosphate group of AEP molecules and some  $\text{Ca}^{2+}$  ions on the particle. The XRD pattern obtained for 1.5% Eu is given on Figure 6. The mean size of the crystallites

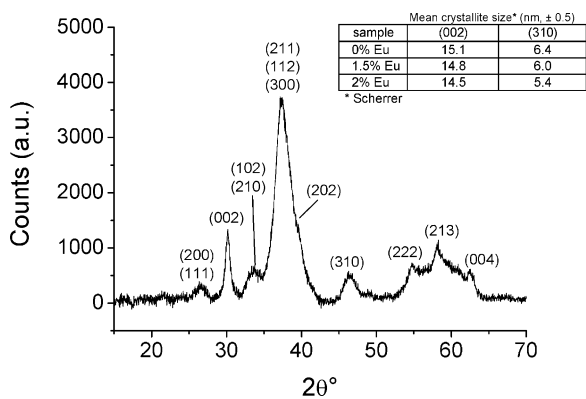


Fig. 6. Typical XRD pattern for apatite-based colloids prepared (at 100 °C) for varying Eu contents. Inset: mean crystallite size from Scherrer's formula.

constitutive of the colloids was also estimated by applying Scherrer's formula to diffraction lines (002) and (310), giving, respectively, a measure of the mean length and width of the nanocrystals as discussed elsewhere.<sup>[22]</sup> The values obtained were added in the inset of Figure 6. As can be seen, the nanocrystalline nature of the colloids is confirmed and the crystallites exhibit dimensions close to 15 nm in length and 6 nm in width/depth.

The mean hydrodynamic radii of the colloids were also determined by way of DLS. In all cases studied, monomodal size distributions were observed. The evolution of the median  $d_{50}$  size parameter was followed for  $T = 80$  °C as a function of the starting AEP content in the solution (Fig. 7). A noticeable decrease in particle size was observed for increasing AEP/Ca starting ratios, with  $d_{50}$  values down to  $46 \pm 5$  nm for AEP/Ca = 0.4 and  $30 \pm 5$  nm for AEP/Ca  $\geq 0.6$ . Interestingly, these two size values are noticeably lower than 100 nm and thus appear suitable for intracellular drug delivery applications.

A decrease in the width of the size distribution, monitored by the polydispersity index (parameter derived from the auto-correlative function of the granulometry data, proportional to the square of the standard deviation of the Gaussian distribution) was also witnessed upon increasing the AEP initial content in the medium (see data on Fig. 7). This observation indicates that the colloids obtained beyond AEP/Ca = 0.4 have an increased homogeneity in particle size, which is also a desirable feature for potential drug nano-carriers.

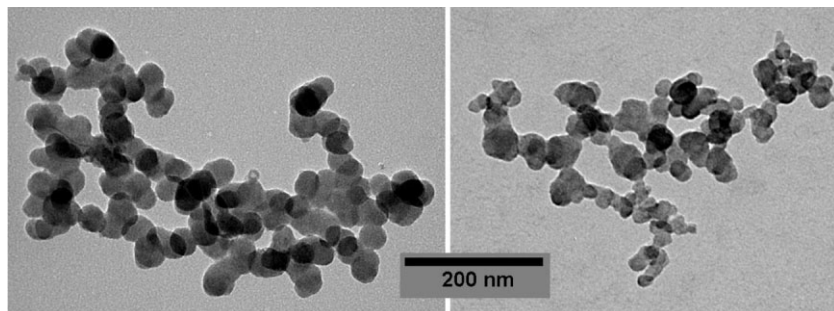


Fig. 8. TEM micrographs on apatite-based colloids (starting AEP/Ca = 1,  $T = 80$  °C).

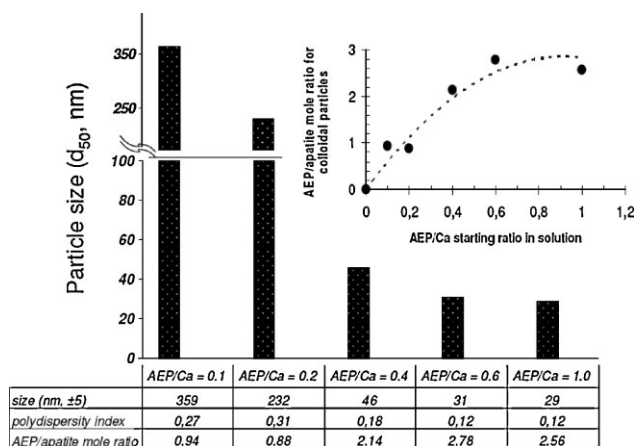


Fig. 7. Evolution of particle size, polydispersity index, and AEP/apatite mole ratio for apatite-based colloids prepared at 80 °C from varying AEP/Ca starting ratios. Inset: evolution of AEP/apatite ratio in colloid versus starting AEP/Ca ratio in solution.

The morphology of the colloids for starting ratios AEP<sub>r</sub>/Ca  $\geq 0.4$  was examined by TEM. A representative example is given in Figure 8 in the case AEP<sub>r</sub>/Ca = 1. The particles were found to exhibit an appreciable morphological homogeneity, with mean sizes in good agreement with the granulometry data (DLS) mentioned above. This homogeneity for AEP<sub>r</sub>/Ca  $\geq 0.4$  suggests the existence of a homogeneous distribution of the AEP molecules on the surface of the apatite nanocrystals.

The amount of AEP grafted on the apatite particles was then followed as a function of the starting AEP/Ca molar ratio (inset of Fig. 7). The obtained curve shows that a stabilization is progressively reached, with an inflexion occurring around AEP/Ca  $\approx 0.6$ . These findings point out the increase of the amount of adsorbed AEP molecules on the apatite crystals up to a maximum value corresponding to ca. 2.7 mol AEP/mol apatite (in our experimental conditions). The attainment of this maximum AEP coverage can then explain the stabilization of the apatite particle size observed beyond AEP/Ca = 0.6.

The above results revealed that a rather strong interaction occurred between AEP molecules and apatite, which is especially clear from the stability of the colloids obtained. This affinity is likely to be linked to the presence of a phosphate end-group on the AEP molecules, which is inclined to interact strongly with calcium phosphate surfaces. This is in agreement with the observation of an IR absorption band at  $754 \text{ cm}^{-1}$  indicative of the formation of  $\text{Ca}(\text{AEP})_2$  complexes. In this context, the ammonium end-groups of AEP molecules would then be exposed toward the solution. The decrease in particle size observed upon increasing the AEP coverage may then be seen as a consequence of electro-steric hindrance effects between adjacent particles, preventing/limiting agglomeration effects. These considerations are in agreement with the positively-charged

agreement with the observation of an IR absorption band at  $754 \text{ cm}^{-1}$  indicative of the formation of  $\text{Ca}(\text{AEP})_2$  complexes. In this context, the ammonium end-groups of AEP molecules would then be exposed toward the solution. The decrease in particle size observed upon increasing the AEP coverage may then be seen as a consequence of electro-steric hindrance effects between adjacent particles, preventing/limiting agglomeration effects. These considerations are in agreement with the positively-charged

particle surface (close to +25 mV) measured by zeta potential measurements, suggesting that the ammonium groups  $-\text{NH}_3^+$  of the AEP molecules are indeed exposed outbound, toward the solution and other particles.

It is interesting to note at this point that the addition of AEP *after* precipitation rather than simultaneously did not lead to any de-agglomeration effect. This is not surprising due to the strong interaction existing between agglomerated apatite nanocrystals in the absence of dispersing agent. It also confirms our conclusions stating that stabilizing molecules such as AEP have to interact with the surface of the crystals during the precipitation process, so as to limit their agglomeration thanks to electro-steric hindrance. In the case of these colloids, the comparison of the mean crystallite size (15 nm in length) estimated from XRD (see Fig. 6) with the hydrodynamic diameters drawn from DLS data ( $\approx 30\text{--}45$  nm for AEP/Ca = 1) suggests that the colloidal nanoparticles are composed of only a few crystallites. In this context, although it is not impossible to find a few AEP molecules entrapped between agglomerated crystallites, the strong decreasing-size effect observed when increasing the AEP content as well as the positive zeta potential are strong indicators of surface modifications of the nanoparticles rather than internal ones. At the alkaline pH ( $\approx 9$ ) used here for the preparation of these apatite colloids, the zeta potential of HA is known to be negative.<sup>[23]</sup> However, the zeta potential, which is generally determined by way of electrophoretic mobility, is only indicative of an overall surface charge summing up all the local contributions. In particular, it does not take into account the presence of local positive centers composed of surface calcium ions that remain accessible to adsorption. The observation of  $\text{Ca}(\text{AEP})_2$  surface complexes in the present work witnesses the possibility to graft AEP molecules (by way of their phosphate group since their positive  $-\text{NH}_3^+$  groups are found to be exposed outbound) onto  $\text{Ca}^{2+}$  surface ions.

Attempts to obtain similar particle sizes by a synthesis protocol performed at neutral pH were not successful as agglomeration remained substantial in this case (leading to particle sizes above 100 nm). A possible explanation for this phenomenon may be related to the more extended hydrated layer on the apatite nanocrystals obtained at pH 7 as compared to pH 9. Indeed, such alkaline media were found<sup>[24]</sup> to lead to apatite compounds exhibiting a chemical composition closer to stoichiometry (decrease of the amount of non-apatitic species). In this context, the nanocrystals prepared at pH 7 are bound to exhibit a larger surface energy for which agglomeration may then interfere to a greater extent with the AEP adsorption process. This hypothesis is supported by the fact that the amount of AEP adsorbed on the apatite particles prepared at pH = 7 is noticeably lower (0.68 mol AEP/mol apatite in the example of the starting ratio AEP<sub>r</sub>/Ca = 0.4) than for pH = 9 (2.14 mol AEP/mol apatite) revealing a much lower degree of interaction between the AEP and apatite crystals. It is however possible

to adjust the pH to physiological value in a subsequent step, after synthesis and dialysis, in order to enable biological applications; and this method should be favored in the objective to minimize agglomeration.

The results reported in this section indicate that it is possible to prepare, from easily handled ionic salts, nano-scale colloids associating biomimetic apatite nanocrystals and a biocompatible phospholipid moiety. Moreover, we showed that the mean particle size for such colloids could be tailored in the range 30–100 nm by modifying synthesis conditions. Applications as intracellular drug-nanocarriers may then be envisioned for these systems.

In addition, a preliminary luminescence study pointed out, in the case of Eu-doped colloids, the typical features of  $\text{Eu}^{3+}$  ions. These results suggest then the possibility to use such luminescent colloids as nanoprobe in view of intracellular applications linked to diagnosis aspects. These considerations are now in development and will be the object of other contributions.

#### *Concluding Remarks*

The data and discussions reported in this contribution were aiming at pointing out several possibilities offered by calcium phosphate apatite-based systems in the field of bio-medical applications. In the form of three selected examples, we addressed adsorption/functionalization processes involving organic molecules of interest, as well as the preparation of Ca–Eu apatite solid solutions, meant to bring new functionalities to apatite materials either as dry bioceramics or as aqueous colloids.

We reported on the possibility to enrich apatite surfaces with risedronate molecules that present potential therapeutic properties for the treatment of osteoporosis. We pointed out in this case the existence of a complex interaction involving not only adsorption but also an exchange with surface ions. We then showed the possibility to convey luminescence properties to apatite crystals prepared by soft chemistry, for example in view of exploring apatite/collagen interfaces through the FRET technique, in order to derive adapted protocols for the preparation of “advanced” biocomposites. Finally, we investigated the preparation of nanometer-scaled apatite-based colloids (with particle size tailorable in the range 30–100 nm), obtained by controlling the agglomeration state of apatite nanocrystals by way of surface grafting of a phospholipid moiety.

The conclusions illustrate some of the numerous potentialities of calcium phosphate apatites in the bio-medical domain, that are progressively widened thanks to a better comprehension of the physico-chemistry of biomimetic apatites and of their surface characteristics allowing to imagine new therapeutic and/or diagnosis perspectives for the future.

- [1] R. Legros, N. Balmain, G. Bonel, *J. Chem. Res. (S)* **1986**, 1, 8.
- [2] a) C. Rey, A. Hina, A. Tofighi, M. J. Glimcher, *Cells Mater.* **1995**, 5, 345; b) S. Cazalbou, C. Combes, D. Eichert, C. Rey, M. J. Glimcher, *J. Bone Miner. Metabol.* **2004**, 22, 310; c) S. Cazalbou, C. Combes, D. Eichert, C. Rey, *J. Mater. Chem.* **2004**, 14, 2148; d) C. Rey, C. Combes, C. Drouet, A. Lebugle, H. Sfihi, A. Barroug, *Materialwiss. Werkstof.* **2007**, 38, 996; e) C. Rey, C. Combes, C. Drouet, H. Sfihi, A. Barroug, *Mater. Sci. Eng, C* **2007**, 27, 198.
- [3] D. Eichert, C. Combes, C. Drouet, C. Rey, *Key Eng. Mater.* **2005**, 284–286, 3.
- [4] W. F. Neuman, T. Y. Toribara, B. J. Mulryan, *J. Am. Chem. Soc.* **1956**, 78, 4263.
- [5] a) R. El Ouenzerfi, N. Kbir-Ariguib, M. Trabelsi-Ayedi, B. Piriou, *J. Lumin.* **1999**, 85, 71; b) R. Ternane, M. Trabelsi-Ayedi, N. Kbir-Ariguib, B. Piriou, *J. Lumin.* **1999**, 81, 165; c) P. Martin, G. Carlot, A. Chevarier, C. Den-Auwer, G. Panczer, *J. Nucl. Mater.* **1999**, 275, 268; d) A. Doat, M. Fanjul, F. Pellé, E. Holland, A. Lebugle, *Biomaterials* **2003**, 24, 3365; e) K. Eun Jin, C. Sung-Woo, H. Seong-Hyeon, *J. Am. Chem. Soc.* **2007**, 90, 2795.
- [6] a) J. E. Davies, *Anat. Rec.* **1996**, 245, 426; b) T. Matsumoto, M. Okazaki, M. Inoue, S. Yamaguchi, T. Kusunose, T. Toyonaga, Y. Hamada, J. Takahashi, *Biomaterials* **2004**, 25, 3807; c) C. J. Wilson, R. E. Cleqq, D. I. Leavesley, M. J. Pearcy, *Tissue Eng.* **2005**, 11, 1.
- [7] a) R. W. Romberg, P. G. Werness, B. L. Riggs, K. G. Mann, *Biochemistry* **1986**, 25, 1176; b) P. V. Hauschka, F. H. Wians, *Anat. Rec.* **1989**, 224, 180; c) A. L. Boskey, W. Ullrich, L. Spevak, H. Gilder, *Calcif. Tissue Int.* **1996**, 58, 45; d) C. Robinson, S. J. Brookes, J. Kirkham, W. A. Bonass, R. C. Shore, *Adv. Dent. Res.* **1996**, 10, 173; e) H. A. Goldberg, K. J. Warner, G. K. Hunter, *Connect. Tissue Res.* **2001**, 42, 25.
- [8] a) V. Hlady, J. Buijs, *Cur. Opin. Biotechnol.* **1996**, 7, 72; b) A. J. Garcia, B. G. Keselowsky, *Crit. Rev. Eukaryot. Gene Expr.* **2002**, 12, 151.
- [9] R. G. Russell, N. B. Watts, F. H. Ebetino, M. J. Rogers, *Osteoporos. Int.* **2008**, 19, 733.
- [10] G. H. Nancollas, R. Tnag, R. J. Phips, Z. Henneman, S. Gulde, W. Wu, A. Mangood, R. G. G. Russel, F. H. Ebetino, *Bone* **2006**, 38, 617.
- [11] G. Charlot, *Chimie Analytique Quantitative*, Masson, Paris, France **1974**.
- [12] a) R. A. M. J. Claessens, Z. I. Kolar, *Langmuir* **1999**, 16, 1360; b) T. Vitha, V. Kubicek, P. Hermann, Z. I. Kolar, H. T. Wolterbeek, J. A. Peters, I. Lukes, *Langmuir* **2008**, 24, **1952**.
- [13] D. L. Andrews, *Chem. Phys.* **1989**, 135, 195.
- [14] D. Fujimoto, T. Moriguchi, *J. Biochem.* **1978**, 83, 863.
- [15] a) R. Ternane, M. Trabelsi-Ayedi, N. Kbir-Ariguib, B. Piriou, *J. Lumin.* **1999**, 81, 165; b) K. Eun Jin, C. Sung-Woo, H. Seong-Hyeon, *J. Am. Chem. Soc.* **2007**, 90, 2795; c) P. Martin, G. Carlot, A. Chevarier, C. Den-Auwer, G. Panczer, *J. Nucl. Mater.* **1999**, 275, 268.
- [16] A. Bartsiakas, A. P. Middleton, *J. Arch. Sci.* **1992**, 19, 63.
- [17] R. D. Shannon, *Acta Cryst.* **1976**, A32, 751.
- [18] a) M. Long, F. Hong, W. Li, F. Li, H. Zhao, Y. Lv, H. Li, F. Hu, L. Sun, C. Yan, Z. Wei, *J. Lumin.* **2008**, 128, 428; b) N. Lakshminarasimhan, U. V. Varadaraju, *J. Solid Status Chem.* **2004**, 177, 3536.
- [19] I. Dos Santos, S. Mazerès, M. Freche, J. L. Lacout, A. M. Sautereau, *Mater. Lett.* **2008**, 62, 4377.
- [20] L. Rothfield, A. Finkelstein, *Ann. Rev. Biochem.* **1968**, 37, 463.
- [21] E. M. Zahidi, *Ph. D. Thesis*, INP Toulouse, France **1984**.
- [22] D. Eichert, D. C. Drouet, H. Sfihi, C. Rey, C. Combes, in: *Biomaterials Research Advances* (Ed.: J. B. Kendall), Nova Science Publishers, New York, USA **2008**, Ch. 5.
- [23] P. Somasundaran, Y. H. C. Wang, in: *Adsorption on and Surface Chemistry of Hydroxyapatite* (Ed.: D. N. Misra), Plenum Press, New York USA **1984**, pp. 129–149.
- [24] C. Drouet, F. Bosc, M. Banu, C. Largeot, C. Combes, G. Dechambre, C. Estournès, G. Raimbeaux, C. Rey, *Powder Technol.* **2009**, 190, 118.